

Received September 1, 2020; revised October 22, 2020; accepted October 23, 2020; date of publication October 29, 2020; date of current version November 16, 2020.

Digital Object Identifier 10.1109/TQE.2020.3034798

Quantum Approximate Optimization With Parallelizable Gates

WOLFGANG LECHNER¹

Institute for Theoretical Physics, University of Innsbruck and Parity Quantum Computing GmbH, 6020 Innsbruck, Austria

This work was supported in part by the Austrian Science Fund (FWF) through a START Grant under Project Y1067-N27 and the SFB BeyondC Project F7108-N38, in part by the Hauser-Raspe Foundation, and the European Union's Horizon 2020 Research and Innovation Program under Grant Agreement 817482, and in part by the Defense Advanced Research Projects Agency under Contract HR001120C0068. This manuscript was submitted to the 2nd International Workshop on Quantum Resource Estimation - QRE2020.

ABSTRACT The quantum approximate optimization algorithm (QAOA) has been introduced as a heuristic digital quantum computing scheme to find approximate solutions of combinatorial optimization problems. We present a scheme to parallelize this approach for arbitrary all-to-all connected problem graphs in a layout of quantum bits (qubits) with nearest-neighbor interactions. The protocol consists of single qubit operations that encode the optimization problem, whereas interactions are problem-independent pairwise CNOT gates among nearest neighbors. This allows for a parallelizable implementation in quantum devices with a planar lattice geometry. The basis of this proposal is a lattice gauge model, which also introduces additional parameters and protocols for QAOA to improve the efficiency.

INDEX TERMS Quantum computing, quantum technology, quantum optimization.

I. INTRODUCTION

With the immense recent developments in quantum technology [1]–[12] the regime of computational quantum advantage is in reach [13]–[15]. Solving computationally hard optimization problems is a possible application of such near-term intermediate-size special purpose quantum computers that currently receives considerable interest. The working principle to solve optimization problems on quantum hardware is to encode the problem in a spin model such that the cost function corresponds to the energy of the system [16]. Finding the ground state of the spin model is thus equivalent to solving the optimization problem. In the seminal paper by Kirkpatrick *et al.* [17], it was shown that hard optimization problems can be mapped to disordered all-to-all connected Ising spin glasses. Due to the large number of local minima, it is computationally challenging to find the ground state of such a model using the current state-of-the-art classical algorithms as in [18]–[20].

The quantum approximate optimization algorithm (QAOA) [21], [22] has been recently introduced as a heuristic digital quantum algorithm to sample approximate ground states using shallow quantum circuits. The scheme consists of a sequence of quantum quenches represented by unitary operators that correspond to a driver Hamiltonian and a problem Hamiltonian, respectively. The number of iterations can be small and angles of each unitary are free

parameters that are optimized via a classical feedback loop. The method has been recently proven to exhibit the optimal Grover speedup in an unstructured search [23]. An open challenge is scalability and programmability to encode arbitrary optimization problems independent of the physical qubit arrangement and connectivity. While larger connectivity can be achieved by a series of swap operations, these operations are problem-dependent and thus difficult to parallelize, which is a limiting factor in scalability and execution speed.

In this article, we present a parallelizable QAOA scheme consisting of nearest-neighbor CNOT gates and single qubit rotations with the aim to solve all-to-all connected combinatorial optimization problems. The scheme is based on the recently introduced encoding of optimization problems in a lattice gauge model (LHZ) [24]. In this mapping, the problem is fully determined by local fields, whereas interactions are uniform and problem-independent. This separation applied to QAOA allows for an implementation with pairwise gates that are executed in parallel on a square lattice with nearest-neighbor connectivity. The required gates consist of three terms: 1) a unitary with local σ_x terms; 2) a unitary that defines the problem with local σ_z terms; and 3) problem-independent interactions consisting of nearest-neighbor CNOT gates and qubit rotations, illustrated in Fig. 1. The mapping also introduces additional free

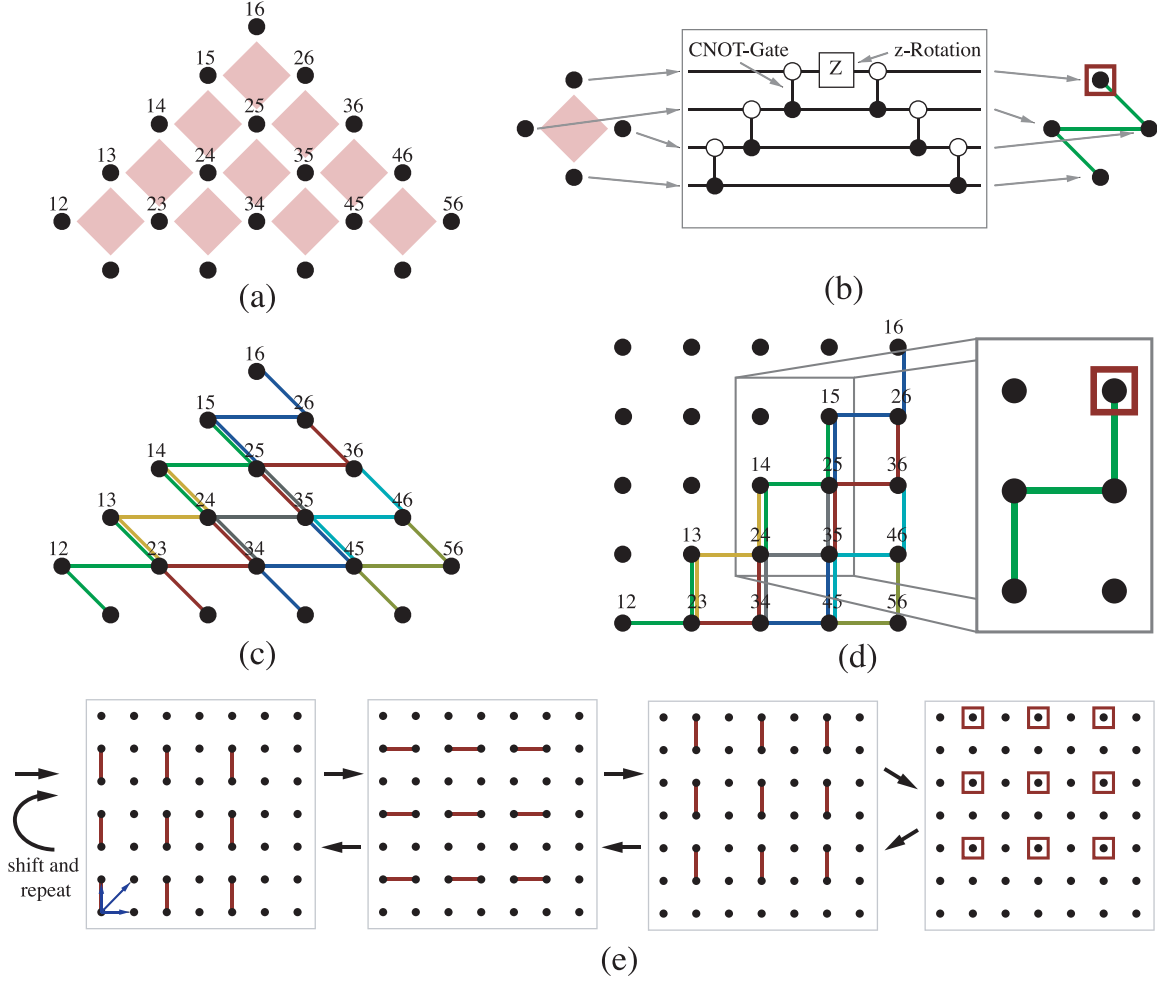


FIGURE 1. (a) Lattice gauge formulation of an all-to-all connected spin model. The z-component of the qubits (dots) represent relative coordinates of two spins i and j (labels) and the optimization problem is encoded in the local fields acting on individual qubits. The interactions are problem-independent four-body interactions on a square lattice (red). (b) QAOA unitary to implement an LHZ plaquette interaction is decomposed into a series of three CNOT gates along a z-shaped path followed by a qubit rotation and three CNOT gates in reversed order back. (c) Pattern of CNOT gates to implement all four-body interactions. (d) System can be realigned to a regular square lattice. In the square lattice, the LHZ four-body plaquette interactions decompose into a sequence of gates that connects two physical plaquettes with CNOT gates (inset, green) and a single R_z -Gate (inset, square) that determines the strength of the constraint. (e) Sequence of parallel CNOT gates (lines) and R_z rotations (squares) to realize all four-body interactions consisting of seven parallel gate operations. The pattern is then shifted up by one row, shifted to the right by one column, and shifted up-and-right (blue arrows) and repeated. Thus, a total number of 28 parallel gates is required to realize all constraints independent of the system size.

parameters and new QAOA protocols that may be used to increase the efficiency of the method.

II. LATTICE GAUGE QAOA

The QAOA [21] aims at finding approximate solutions in a hybrid quantum-classical approach inspired by quantum annealing [25]–[29]. In quantum annealing, the ground state of the problem Hamiltonian is prepared by an adiabatic sweep of the form such as $H(t) = \frac{t_{\max}-t}{t_{\max}}H_0 + \frac{t}{t_{\max}}H_p$, where $H_0 = \sum_i \sigma_x^{(i)}$ is the driver Hamiltonian, and $H_p = \sum_{i<j} J_{ij} \sigma_z^{(i)} \sigma_z^{(j)}$ is the problem Hamiltonian. The system is initially prepared in the ground state of H_0 . Given that t_{\max} is large compared to the minimum spectral gap in the time-dependent spectrum the system will remain close to the instantaneous ground

state, and thus, the system is found close to the ground state of H_p at time t_{\max} . It is an open question whether a quantum speedup for hard combinatorial problems can be expected with this protocol [27], [28].

In QAOA, instead of adiabatically transforming the Hamiltonian, the system is sequentially quenched, e.g., with

$$|\psi(m, \beta_1, \gamma_1, \dots)\rangle = U_x(\beta_1)U_p(\gamma_1) \dots U_x(\beta_m)U_p(\gamma_m)|s\rangle. \quad (1)$$

Here, $|s\rangle$ is the initial state, which is typically chosen to be the equal superposition in computational basis $|s\rangle = \frac{1}{\sqrt{2^N}} \sum |z\rangle$ and the unitary operators

$$U_x(\beta) = e^{-i\beta H_0} = \prod_{i=1}^N e^{-i\beta \sigma_x^{(i)}} \quad (2)$$

and

$$U_p(\gamma) = e^{-i\gamma H_p}. \quad (3)$$

The number of iteration cycles m as well as β_i and γ_i are free parameters that are tuned to minimize the expectation of the final state with respect to the problem Hamiltonian

$$E = \min_{\gamma, \beta} \langle \psi | H_p | \psi \rangle. \quad (4)$$

This parameter optimization is done via a hybrid quantum-classical algorithm where the state $|\psi\rangle$ is prepared using the quantum device and the parameters are updated as classical feedback from the outcome of measurements. We note that the digital implementation of the optimization algorithm also allows for encoding nonquadratic problems with higher order terms. For optimization problem, one might be interested in the probability to find the best solution, which is measured by the ground-state fidelity

$$F = |\langle \psi | \varphi_0 \rangle|. \quad (5)$$

Here, $|\varphi_0\rangle$ is the ground-state of H_p . Note that in the context of classical optimization problems, a practical measure is the energy of the final state rather than the fidelity. The energy is well defined also for degenerate ground-states. Also, classical optimization does in principle not require large overlap with the ground-state but only finite overlap. Here, we chose the ground-state fidelity as a general measure for reachability of the ground-state. The challenge that we address here is the implementation of U_p , which consists of geometrically nonlocal terms that can, in general, not be mapped directly to the physical qubit layout.

The nonlocal and disordered interactions can be removed with the recently introduced LHZ mapping [24], which is a lattice gauge formulation for optimization problems. The LHZ-Hamiltonian has the form [30]–[35]

$$H(t) = H_0(t) + H_p(t), \text{ where} \quad (6)$$

$$H_0(t) = A(t) \sum_i^K \sigma_x^{(i)} \quad (7)$$

$$H_p(t) = B(t) \sum_i^K J_i \sigma_z^{(i)} + C(t) \sum_{l=1}^{K-N+1} C_l \sigma_z^{(l,n)} \sigma_z^{(l,e)} \sigma_z^{(l,s)} \sigma_z^{(l,w)}. \quad (8)$$

Here, $K = N(N-1)/2$ is the number of connections in the graph and the indices n, e, s, w denote north, east, south, and west qubit of each plaquette. The schedule function A is switched from 1 to 0 and B and C are switched from 0 to 1, respectively. The physical qubits represent the relative orientation of the spins in the optimization problem. Thus, the number of physical qubits is the number of edges in the problem graph, which introduces a quadratic overhead for general all-to-all models. The matrix elements J_i that encode the optimization problem are, in contrast to the spin model,

local fields acting on single qubits. A third, additional term is introduced that energetically constrains the system in the increased Hilbert space to the low energy subspace. The constraints are four-body interactions acting on plaquettes [see Fig. 1(a)] of a square lattice.

Using the above mapping in the spirit of QAOA suggests the following unitary operators as building blocks for the optimization algorithm:

$$U_x(\beta) = \prod_{i=1}^K e^{-i\beta \sigma_x^{(i)}} \quad (9)$$

$$U_z(\gamma) = \prod_{i=1}^K e^{-i\gamma J_i \sigma_z^{(i)}} \text{ and} \quad (10)$$

$$U_C(\Omega) = \prod_{l=1}^{K-N+1} e^{-i\Omega C_l \sigma_z^{(l,n)} \sigma_z^{(l,e)} \sigma_z^{(l,s)} \sigma_z^{(l,w)}}. \quad (11)$$

The unitary U_x is the propagator of the driver Hamiltonian. The problem Hamiltonian is now split into two parts, U_z and U_C . In the latter, C_l are the constraint strengths of each plaquette l . The constraint strengths are free parameters because the low energy subspace is gauge invariant under change in C_l . Note that C_l is a single parameter and for each plaquette identical. They can be optimized in addition to the angles β , γ , Ω . With the separation of interactions and local fields, the terms in U_z and U_x are all simple single qubit rotations and phase rotations. The only programmable (and therefore disordered) Hamiltonian is U_z . The remaining term containing the interactions (i.e., U_C) is problem-independent. Due to this independence of interactions and encoded problem the two-qubit gates are uniform and in the following a parallelizable implementation is discussed.

The four-body interactions required in U_C are problem independent and thus identical for each plaquette. These individual plaquette terms can be realized as shown in Fig. 1(b) using six CNOT gates and one qubit rotation R_z . The CNOT gates are performed along a *path* connecting all four qubits, followed by a qubit rotation is performed followed by the same CNOT gates performed in reverse order. We have chosen the particular z-shaped path as shown in Fig. 1(b). Note that other *paths*, e.g., clockwise along a plaquette is also possible. Plugging this gate sequence into the LHZ architecture results in the particular connectivity graph, as shown in Fig. 1(c). By realignment to a regular square graph, the CNOT gates act on nearest neighbors only [see Fig. 1(d)]. Note that the plaquette interactions in LHZ translate to a sequence of CNOT gates along lines that connect two plaquettes in the physical graph [see Fig. 1(d) (right)]. As these interactions are identical for each plaquette, they can be executed in parallel. Fig. 1(e) shows a sequence with parallel gates consisting of three particular CNOT gates, an R_z gate, and the three CNOT gates in reversed order. To reach all plaquettes, this sequence is repeated in total four times, where after each run the gates are shifted by one row, one

column, and one row-and-column. This makes in total 28 parallel gates to implement all constraints.

Note that the strength of the constraints C_l is determined by the R_Z -Gate alone and that the CNOT gates are independent of the problem and also independent of the constraints. Thus, only local Z operations contain disorder and all CNOT gates are problem-independent and parallelizable on a 2-D grid.

III. PARAMETER AND PROTOCOL OPTIMIZATION

QAOA is a feedback-driven algorithm [21]. The feedback consists of measuring the outcome of quenches according to a protocol in (1) on the quantum device and using classical optimization methods to improve the parameters β_i, γ_i in (2). In the protocol presented here, the unitary operators given in (9)–(11) introduce additional free parameters (Ω_i and C_l) and additional quench protocols. In the following we address the question, how these additional degrees of freedom can be used to improve the algorithm.

The unitary operators (9)–(11) allow for two possible algorithmic directions of improvement: 1) the protocol that determines the order and form of the operators; and 2) the choice of parameters that are varied. In order to compare the different approaches, we keep the number of feedback iterations m fixed as this is the limiting factor in the experiment. The initial state is chosen to be the uniform superposition in the computational basis and the unitary operations are denoted as $|\psi\rangle = U_{a,b,c}|s\rangle$. We consider for illustration three particular protocols

$$U_a = U_p(\gamma_0)U_x(\beta_1)U_p(\gamma_1) \dots \quad (12)$$

$$U_b = U_z(\gamma_0)U_c(\Omega_0)U_x(\beta_1)U_z(\gamma_1)U_c(\Omega_1) \dots \quad (13)$$

$$U_c = U_z(\gamma_0)U_c(\Omega_0, C_l)U_x(\beta_1)U_z(\gamma_1)U_c(\Omega_1, C_l) \dots \quad (14)$$

Here, protocol U_a is a sequence of applying the LHZ problem Hamiltonian with $U_p = e^{-i\gamma H_p}$ and the driver Hamiltonian. Protocol U_b makes use of the splitting between local field terms and interaction terms and optimizes the parameters β, Ω , and γ independently. Protocol U_c also includes an update of the constraint strengths and thus the Hamiltonian itself.

We consider an optimization problem encoded in $K = 6$ qubits arranged on a square lattice with three plaquettes. The parameters are optimized using the following Monte Carlo procedure.

- 1) The parameters are initialized with $\gamma_i, \beta_i, \Omega_i = 1$ and $C_l = 2$. The interaction matrix is chosen randomly from the interval $J_{ij} \in \{-1, \dots, 1\}$.
- 2) The final states $|\psi\rangle$ are prepared according to the above protocols U_a, U_b , and U_c .
- 3) The expectation E and the fidelity F are determined.
- 4) This is repeated $M = 4000$ times and in each Monte Carlo step, a randomly chosen parameter is updated by a random number in the range $\delta = \{-1, \dots, 1\}$. The set of parameters is accepted if the expectation

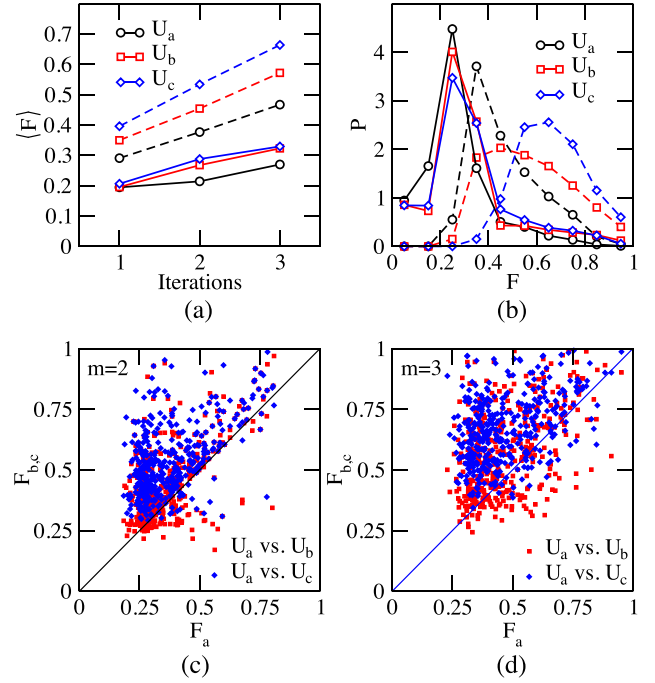


FIGURE 2. (a) Average fidelity defined as overlap of the final state with the ground-state of the problem Hamiltonian as a function of number of iteration cycles. Average is taken over $L = 400$ random instances optimizing F (dashed) and $L = 2000$ instances optimizing the expectation E (solid). QAOA with driver and problem Hamiltonian (protocol U_a , black) improves with the number of iterations. Separation of the problem Hamiltonian (protocol U_b , red) and optimizing also the constraints (protocol U_c , blue) improves the fidelity for all m , the number of iterations. (b) Normalized histogram P of the fidelity for the same parameters as in panel (a) with $m = 3$ iterations optimizing the expectation (solid) and the fidelity (dashed). (c) Scatter plot of the fidelity optimization with the same parameters as in panel (a) with $m = 2$ iterations comparing direct fidelity optimization with protocol U_a against protocol U_b (red) and against protocol U_c (blue), respectively. (d) Scatter plot of the fidelity comparing protocols as in panel (c) with $m = 3$ iteration cycles.

E decreases and rejected otherwise. For comparison we also optimized parameters directly improving the fidelity F . In this case, the update is accepted if the fidelity increases.

- 5) This procedure is repeated for random instances of J_{ij} . The averages are taken over $L = 2000$ realizations. The three protocols U_a, U_b , and U_c are compared using the same instances for numbers of iteration $m = 1, 2$, and 3. In protocol U_c , the update of C_l is attempted every tenth steps.

Fig. 2 depicts the fidelity in comparison for protocols U_a, U_b , and U_c [see Fig. 2(a)]. In the context of QAOA, the separation of local field terms and interaction terms results in a tradeoff between the number of qubits and the number of CNOT gates. In the standard encoding, the number of qubits is smaller but due to the required SWAP operations the number of CNOT gates is larger. The advantages and disadvantages of more qubits but less CNOT gates have to be analyzed for each implementation individually. The

additional optimization of constraints using protocol U_c does further improve the fidelity. Note that this protocol may result in a further improvement if more measurements are used. The histograms of the fidelities for the various protocols show that protocol U_c has the best average performance and also the largest contributions for fidelities close to $F = 1$ [see Fig. 2(b)]. A direct comparison of protocols [see Fig. 2(c) and (d)] show that most instances result in a lower fidelity using protocol U_a compared with the optimal protocol U_c .

IV. CONCLUSION AND OUTLOOK

We have applied the LHZ mapping to QAOA, which allows one to separate the two-qubit gates from the programmable local fields containing the optimization problem. With this separation, we introduce a scheme with full parallelization of gates on the quantum device. The optimization problem is solved with problem-independent CNOT gates that can be performed in parallel on a square lattice, whereas only local fields are problem dependent, which is directly applicable to qubits on a 2-D grid [14]. The mapping also suggests several novel QAOA protocols, in particular optimization of local fields independent of the optimization of interactions. Using Monte Carlo as an optimization technique and comparing three particular protocols with the fixed number of readouts, we find that for the given instances the best protocol is to use the unitary operators as given in (9)–(11) and an update of the angles and gauge constraints. Note that the depicted geometry in Fig. 1 corresponds to an all-to-all graph. The layout represents a restricted Boltzmann machine if the full square lattice is filled, a mapping that could be directly applicable for unsupervised machine learning applications [9].

The system sizes considered in the work are not sufficient to make decisive statements about the scaling of the presented method. In particular, the main advantages may arise from the simplified implementation with its intrinsic parallelizability. Thus an important step will be the experimental implementation. As a future direction, the parallelizable QAOA scheme may be extended to more complex driver Hamiltonians, e.g., nonstoquastic terms [36]–[38].

ACKNOWLEDGMENT

Any opinions, findings and conclusions or recommendations expressed in this material are those of the author(s) and do not necessarily reflect the views of DARPA.

REFERENCES

- [1] J. I. Cirac and P. Zoller, "Goals and opportunities in quantum simulation," *Nat. Phys.*, vol. 8, no. 4, pp. 264–266, 2012, doi: [10.1038/nphys2275](#).
- [2] I. Georgescu, S. Ashhab, and F. Nori, "Quantum simulation," *Rev. Mod. Phys.*, vol. 86, no. 1, pp. 153–185, 2014, doi: [10.1103/RevModPhys.86.153](#).
- [3] A. Wallraff *et al.*, "Strong coupling of a single photon to a superconducting qubit using circuit quantum electrodynamics," *Nature*, vol. 431, no. 7005, pp. 162–167, 2004, doi: [10.1038/nature02851](#).
- [4] J. Koch *et al.*, "Charge-insensitive qubit design derived from the Cooper pair box," *Phys. Rev. A*, vol. 76, no. 4, 2007, Art. no. 042319, doi: [10.1103/PhysRevA.76.042319](#).
- [5] R. Blatt and C. F. Roos, "Quantum simulations with trapped ions," *Nat. Phys.*, vol. 8, no. 4, pp. 277–284, 2012, doi: [10.1038/nphys2252](#).
- [6] I. Bloch, J. Dalibard, and S. Nascimbene, "Quantum simulations with ultracold quantum gases," *Nat. Phys.*, vol. 8, no. 4, pp. 267–276, 2012, doi: [10.1038/nphys2259](#).
- [7] A. A. Houck, H. E. Türeci, and J. Koch, "On-chip quantum simulation with superconducting circuits," *Nat. Phys.*, vol. 8, no. 4, pp. 292–299, 2012, doi: [10.1038/nphys2251](#).
- [8] S. Bravyi, D. Gosset, and R. König, "Quantum advantage with shallow circuits," *Science*, vol. 362, no. 6412, pp. 308–311, 2018, doi: [10.1126/science.aar3106](#).
- [9] J. Otterbach *et al.*, "Unsupervised machine learning on a hybrid quantum computer," 2017, *arXiv:1712.05771*.
- [10] H. Bernien *et al.*, "Probing many-body dynamics on a 51-atom quantum simulator," *Nature*, vol. 551, no. 7682, pp. 579–584, 2017, doi: [10.1038/nature24622](#).
- [11] T. Watson *et al.*, "A programmable two-qubit quantum processor in silicon," *Nature*, vol. 555, no. 7698, pp. 633–637, 2018, doi: [10.1038/nature25766](#).
- [12] J. Zhang *et al.*, "Observation of a many-body dynamical phase transition with a 53-qubit quantum simulator," *Nature*, vol. 551, no. 7682, pp. 601–604, 2017, doi: [10.1038/nature24654](#).
- [13] J. Preskill, "Quantum computing in the NISQ era and beyond," *Quantum*, vol. 2, 2018, Art. no. 79, doi: [10.22331/q-2018-08-06-79](#).
- [14] S. Boixo *et al.*, "Characterizing quantum supremacy in near-term devices," *Nat. Phys.*, vol. 14, no. 6, pp. 595–600, 2018, doi: [10.1038/s41567-018-0124-x](#).
- [15] A. W. Harrow and A. Montanaro, "Quantum computational supremacy," *Nature*, vol. 549, no. 7671, pp. 203–209, 2017, doi: [10.1038/nature23458](#).
- [16] A. Lucas, "Ising formulations of many NP problems," *Front. Phys.*, vol. 2, 2014, Art. no. 5, doi: [10.3389/fphy.2014.00005](#).
- [17] S. Kirkpatrick, C. D. Gelatt, and M. P. Vecchi, "Optimization by simulated annealing," *Science*, vol. 220, no. 4598, pp. 671–680, 1983, doi: [10.1126/science.220.4598.671](#).
- [18] L. Ingber, "Simulated annealing: Practice versus theory," *Math. Comput. Model.*, vol. 18, no. 11, pp. 29–57, 1993, doi: [10.1016/0895-7177\(93\)90204-C](#).
- [19] W. Wang, J. Machta, and H. G. Katzgraber, "Comparing Monte Carlo methods for finding ground states of Ising spin glasses: Population annealing, simulated annealing, and parallel tempering," *Phys. Rev. E*, vol. 92, Jul. 2015, Art. no. 013303, doi: [10.1103/PhysRevE.92.013303](#).
- [20] B. Heim, T. F. Rønnow, S. V. Isakov, and M. Troyer, "Quantum versus classical annealing of Ising spin glasses," *Science*, vol. 348, no. 6231, pp. 215–217, 2015, doi: [10.1126/science.aaa4170](#).
- [21] E. Farhi, J. Goldstone, and S. Gutmann, "A quantum approximate optimization algorithm," 2014, *arXiv:1411.4028*.
- [22] E. Farhi and A. W. Harrow, "Quantum supremacy through the quantum approximate optimization algorithm," 2016, *arXiv:1602.07674*.
- [23] Z. Jiang, E. G. Rieffel, and Z. Wang, "Near-optimal quantum circuit for Grover's unstructured search using a transverse field," *Phys. Rev. A*, vol. 95, Jun. 2017, Art. no. 062317, doi: [10.1103/PhysRevA.95.062317](#).
- [24] W. Lechner, P. Hauke, and P. Zoller, "A quantum annealing architecture with all-to-all connectivity from local interactions," *Sci. Adv.*, vol. 1, no. 9, 2015, Art. no. e1500838, doi: [10.1126/sciadv.1500838](#).
- [25] T. Kadowaki and H. Nishimori, "Quantum annealing in the transverse Ising model," *Phys. Rev. E*, vol. 58, pp. 5355–5363, Nov. 1998, doi: [10.1103/PhysRevE.58.5355](#).
- [26] E. Farhi, J. Goldstone, S. Gutmann, and M. Sipser, "Quantum computation by adiabatic evolution," 2000, *arXiv:quant-ph/0001106*.
- [27] T. Albash and D. A. Lidar, "Adiabatic quantum computation," *Rev. Mod. Phys.*, vol. 90, Jan. 2018, Art. no. 015002, doi: [10.1103/RevModPhys.90.015002](#).
- [28] S. Boixo *et al.*, "Evidence for quantum annealing with more than one hundred qubits," *Nat. Phys.*, vol. 10, no. 3, pp. 218–224, Mar. 2014, doi: [10.1038/nphys2900](#).
- [29] S. Boixo *et al.*, "Computational multiqubit tunnelling in programmable quantum annealers," *Nat. Commun.*, vol. 7, Jan. 2016, Art. no. 10327, doi: [10.1038/ncomms10327](#).
- [30] A. Rocchetto, S. C. Benjamin, and Y. Li, "Stabilizers as a design tool for new forms of the Lechner-Hauke-Zoller annealer," *Sci. Adv.*, vol. 2, no. 10, 2016, Art. no. e1601246, doi: [10.1126/sciadv.1601246](#).

- [31] T. Albash, W. Vinci, and D. A. Lidar, "Simulated-quantum-annealing comparison between all-to-all connectivity schemes," *Phys. Rev. A*, vol. 94, no. 2, 2016, Art. no. 022327, doi: [10.1103/PhysRevA.94.022327](https://doi.org/10.1103/PhysRevA.94.022327).
- [32] F. Pastawski and J. Preskill, "Error correction for encoded quantum annealing," *Phys. Rev. A*, vol. 93, no. 5, 2016, Art. no. 052325, doi: [10.1103/PhysRevA.93.052325](https://doi.org/10.1103/PhysRevA.93.052325).
- [33] S. Puri, C. K. Andersen, A. L. Grimsmo, and A. Blais, "Quantum annealing with all-to-all connected nonlinear oscillators," *Nat. Commun.*, vol. 8, 2017, Art. no. 15785, doi: [10.1038/ncomms15785](https://doi.org/10.1038/ncomms15785).
- [34] M. Leib, P. Zoller, and W. Lechner, "A transmon quantum annealer: Decomposing many-body Ising constraints into pair interactions," *Quantum Sci. Technol.*, vol. 1, no. 1, 2016, Art. no. 015008, doi: [10.1088/2058-9565/1/1/015008](https://doi.org/10.1088/2058-9565/1/1/015008).
- [35] A. W. Glaetzle, R. M. van Bijnen, P. Zoller, and W. Lechner, "A coherent quantum annealer with Rydberg atoms," *Nat. Commun.*, vol. 8, 2017, Art. no. 15813, doi: [10.1038/ncomms15813](https://doi.org/10.1038/ncomms15813).
- [36] S. Bravyi, D. P. Divincenzo, R. I. Oliveira, and B. M. Terhal, "The complexity of stoquastic local Hamiltonian problems," 2006, *arXiv:quant-ph/0606140*.
- [37] H. Nishimori and K. Takada, "Exponential enhancement of the efficiency of quantum annealing by non-stoquastic Hamiltonians," *Front. ICT*, vol. 4, 2017, Art. no. 2, doi: [10.3389/fict.2017.00002](https://doi.org/10.3389/fict.2017.00002).
- [38] L. Hormozi, E. W. Brown, G. Carleo, and M. Troyer, "Nonstoquastic Hamiltonians and quantum annealing of an Ising spin glass," *Phys. Rev. B*, vol. 95, no. 18, 2017, Art. no. 184416, doi: [10.1103/PhysRevB.95.184416](https://doi.org/10.1103/PhysRevB.95.184416).